The Cryosphere Discuss., 6, 1157–1180, 2012
www.the-cryosphere-discuss.net/6/1157/2012/
doi:10.5194/tcd-6-1157-2012

The Cryosphere Discussions

3-D image-based numerical computations of snow permeability: links to specific surface area, density, and microstructural anisotropy

N. Calonne[1,2], C. Geindreau[2], F. Flin[1], S. Morin[1], B. Lesaffre[1], S. Rolland du Roscoat[2], and P. Charrier[2]

[1]Météo-France – CNRS, CNRM-GAME URA1357, CEN, Grenoble, France
[2]Université Joseph Fourier Grenoble 1 – Grenoble INP – CNRS, 3S-R UMR5521, Grenoble, France

Received: 2 March 2012 – Accepted: 6 March 2012 – Published: 19 March 2012

Correspondence to: N. Calonne (neige.calonne@meteo.fr), C. Geindreau (christian.geindreau@hmg.inpg.fr), F. Flin (frederic.flin@meteo.fr)

Published by Copernicus Publications on behalf of the European Geosciences Union.

Abstract

We used three-dimensional (3-D) images of snow microstructure to carry out numerical estimations of the full tensor of the intrinsic permeability of snow (**K**). This study was performed on 35 snow samples, spanning a wide range of seasonal snow types. Because the permeability is related to a characteristic length, we introduced a dimensionless tensor $\mathbf{K}^* = \mathbf{K}/r_{es}^2$, where the equivalent sphere radius of ice grains (r_{es}) is computed from the specific surface area of snow (SSA) and the ice density (ρ_i) as follows: $r_{es} = 3/(\mathrm{SSA} \times \rho_i)$. Values of K^*, the average of vertical and horizontal components of $\mathbf{K}^*$, were plotted vs. snow density (ρ_s) and compared to analytical models and data from the literature, showing generally a good agreement. The 35 values of K^* were fitted to ρ_s and provide the following regression: $K^* = 2.94 \times \exp(-0.013\rho_s)$, with a correlation coefficient of 0.985. This indicates that permeability, if assumed isotropic, can be reasonably determined from SSA and ρ_s, which are both easily measurable in the field. However, the anisotropy coefficient of **K**, induced by the snow microstructure, ranges from 0.74 to 1.66 for the samples considered. This behavior is consistent with that of the effective thermal conductivity obtained in a previous work.

1 Introduction

Once fallen on the ground, snow forms a complex porous material made of ice, air, water vapor and sometimes liquid water. The amount of these quantities, and their geometrical arrangement at the grains scale, referred to as the microstructure, strongly influence the physical properties of snow. Among them, the intrinsic permeability tensor of snow **K** (m^2) links the pressure gradient $\boldsymbol{\nabla} p$ ($\mathrm{Pa\,m^{-1}}$) and the discharge per unit area **q** ($\mathrm{m\,s^{-1}}$) through the Darcy's law $\mathbf{q} = -(1/\mu)\mathbf{K}\boldsymbol{\nabla} p$, where μ is the dynamic viscosity of the fluid ($\mathrm{kg\,m^{-1}\,s^{-1}}$).

The intrinsic permeability is of particular interest to better understand the transport properties of snow and firn, such as wind pumping (Colbeck, 1989, 1997), convection

TCD
6, 1157–1180, 2012

(Akitaya, 1974; Powers et al., 1985; Brun and Touvier, 1987; Sturm and Johnson, 1991; Albert et al., 2004) and liquid water flow (Colbeck, 1975, 1976; Waldner et al., 2004; Katsushima et al., 2009; Yamaguchi et al., 2010). It is a key variable for a wide number of applications such as atmospheric and firn chemistry (Freitag et al., 2002; Neumann, 2003; Grannas et al., 2007) or snow-firn metamorphism (Albert, 2002; Hörhold et al., 2009). Recently, permeability has also been proposed as a means of characterization for quantitative snow classification (Arakawa et al., 2009).

The first quantitative data on snow permeability are attributed to Bader (1939). Shimizu (1970), Sommerfeld and Rocchio (1993), and Jordan et al. (1999) realized extensive experiments on seasonal snow and proposed parametrizations depending on grain size and density. However, these studies are characterized by a significant scatter in the results, which seems mainly due to experimental reasons (Sommerfeld and Rocchio, 1993). More recently, the availability of 3-D images of snow and firn from X-ray tomography (Brzoska et al., 1999; Coléou et al., 2001; Freitag et al., 2004; Schneebeli and Sokratov, 2004; Kaempfer et al., 2005) opened the way to numerical simulations. Courville et al. (2010) computed one component of the permeability of firn samples using Lattice-Boltzman modeling and Zermatten et al. (2011) performed direct pore-level simulations on five snow samples. While these numerical computations seem particularly promising, the obtained results show only a relative agreement with previous experimental studies and theoretical models.

To try to better understand the origin of the scatter observed in the literature and the impact of the snow microstructure, we carried out numerical simulations of the intrinsic permeability (**K**) on 35 3-D images of snow obtained from microtomography. Computations were performed with the software Geodict (Thoemen et al., 2008; Koivu et al., 2009; Calonne et al., 2011) and are based on the periodic homogenization method (Auriault et al., 2009). This work follows the pioneering developments of Courville et al. (2010) and Zermatten et al. (2011). The main differences lie in the fact that our study considers a wide range of snow types and samples, uses the periodic homogenization method and evaluates the anisotropy of **K**. In addition, detailed comparisons to

TCD
6, 1157–1180, 2012

the main datasets and analytical laws available in the literature are provided and discussed.

2 Methods

2.1 Snow samples

Numerical computations were performed on 35 tomographic images obtained from previous experiments or field sampling, spanning most snow types of seasonal snow, i.e. Precipitation Particles (PP), Decomposing and Fragmented precipitation particles (DF), Rounded Grains (RG), Faceted Crystals (FC), Depth Hoar (DH) and Melt Forms (MF), according to the International Classification for Seasonal Snow on the Ground (ICSSG) (Fierz et al., 2009).

Two-thirds of the snow samples come from controlled cold-room experiments: a first series (PP, DF and RG) was obtained by subjecting deposited natural snow to isothermal conditions at 271 K (Flin et al., 2004). Another RG sample was obtained under similar conditions, but after sieving. A second series (RG, FC and DH) was obtained under a temperature gradient of 43 $K\,m^{-1}$ at 269 K and corresponds to various stages of metamorphism of the initial sieved snow (RG) into FC then DH. Two others similar experiments, with a gradient of 16 and 100 $K\,m^{-1}$ at 268 and 270 K, provided two samples (FC and DH) (Coléou et al., 2001; Flin and Brzoska, 2008). A series of MF samples was obtained by grain coarsening in water-saturated snow using the method of Raymond and Tusima (1979) followed by draining of their liquid water content (Coléou et al., 2001; Flin et al., 2011).

The remaining snow samples were directly collected in the field: 10 snow specimens (PP, DF and RG) were sampled at increasing depths in the snowpack of the Girose glacier (Écrins, French Alps) (Flin et al., 2011). Another PP sample was collected at Col de Porte (Chartreuse, French Alps).

TCD
6, 1157–1180, 2012

Additional information about the snow samples are indicated in Table 1 of the auxiliary materials available online.

2.2 Computations of snow permeability

Physical phenomena in heterogeneous systems such as porous media can be modeled by an equivalent continuous macroscopic description, provided that the condition of separation of scales is satisfied (Auriault, 1991; Auriault et al., 2009). This fundamental condition may be expressed as $\varepsilon = l/L << 1$, in which l and L are the characteristic lengths of the heterogeneities at the pore scale and of the macroscopic sample or excitation, respectively. This condition implies the existence of a Representative Elementary Volume (REV) of size l of the material and the physical phenomena. The REV constitutes the smallest fraction of the sample volume from which a variable representative of the whole can be determined. Assuming that this condition is fulfilled, the main results concerning the derivation of Darcy's law from the physics at the pore scale using the homogenization method for periodic structures (Ene and Sanchez-Palencia, 1975; Auriault, 1991), are presented.

Without loss of generality (Auriault, 2011), we consider a rigid porous matrix which is periodic with period Ω, i.e. the size of the REV, and which is fully saturated by an incompressible Newtonian fluid of density ρ and viscosity μ. Ω^s and Ω^f are the domains occupied by the solid and the fluid, respectively. The common boundary of Ω^s and Ω^f is denoted Γ. The porosity is defined as $\phi = |\Omega^f|/|\Omega|$. At the pore scale, the steady state flow is described by:

$$\mu\Delta\mathbf{v} - \boldsymbol{\nabla} p = \rho(\mathbf{v}\cdot\boldsymbol{\nabla})\mathbf{v}, \qquad \boldsymbol{\nabla}\cdot\mathbf{v} = 0, \qquad \text{within } \Omega^f, \qquad \text{with } \mathbf{v} = \mathbf{0} \text{ on } \Gamma \tag{1}$$

where $\mathbf{v}$ and p are the velocity and the pressure of the fluid, respectively. Using the homogenization method, it can be shown that the corresponding macroscopic description strongly depends on the order of magnitude of the pore Reynolds number, $R_{el} = |\rho(\mathbf{v}\cdot\boldsymbol{\nabla})\mathbf{v}|/|\mu\Delta\mathbf{v}| = \mathcal{O}(\rho v_c l/\mu)$ where v_c is a characteristic value of fluid velocity.

TCD
6, 1157–1180, 2012

When $R_{el} < \mathcal{O}(1)$, the macroscopic flow is described by Darcy's law, otherwise non-linearities appear at the macroscopic scale (Mei and Auriault, 1991). In what follows, it is assumed that $R_{el} < \mathcal{O}(1)$, which is typically the case for example if we consider air-flow through snow and firn induced by moderate winds ($< 6\,\mathrm{m\,s^{-1}}$) over the snowpack surface (Albert, 2002). Under such conditions, the macroscopic description is written:

$$\langle \mathbf{v} \rangle = -\frac{\mathbf{K}}{\mu} \boldsymbol{\nabla} p, \qquad \boldsymbol{\nabla} \cdot \langle \mathbf{v} \rangle = 0, \qquad \text{with } \langle \mathbf{x} \rangle = \frac{1}{\Omega} \int_{\Omega^{\mathrm{f}}} \mathbf{x} \, \mathrm{d}\Omega \tag{2}$$

where $\langle \mathbf{v} \rangle = \mathbf{q}$ represents the Darcy's velocity and $\mathbf{K}$ is the intrinsic permeability tensor of the porous media. This tensor, which is symmetric and positive, is defined as $K_{ij} = \langle k_{ij} \rangle$. The second order tensor $\mathbf{k}$ is solution of the following boundary value problem over the REV,

$$\mu \Delta \mathbf{v} - \boldsymbol{\nabla} \tilde{p} - \boldsymbol{\nabla} p = \mathbf{0}, \qquad \boldsymbol{\nabla} \cdot \mathbf{v} = 0, \qquad \text{within } \Omega^{\mathrm{f}}, \qquad \text{with } \mathbf{v} = \mathbf{0} \text{ on } \Gamma \tag{3}$$

where $\mathbf{v} = -(1/\mu)\mathbf{k}\boldsymbol{\nabla} p$, the pressure fluctuation $\tilde{p}$ (with $\langle \tilde{p} \rangle = 0$) are the periodic unknowns and $\boldsymbol{\nabla} p$ is a given macroscopic gradient of pressure.

The components of the permeability tensor $\mathbf{K}$ were estimated by solving the above boundary value problem (3) on a REV extracted from tomographic images (see Sect. 3.4), using the software Geodict (http://www.geodict.de). It was previously ensured that the ratio between closed and open porosity is negligible, meaning that it is correct to consider that air can flow through the whole porosity of REVs. In the following, the non-diagonal terms of the tensor $\mathbf{K}$, about 50 times lower than diagonal terms, are not presented (the x, y and z axes of 3-D images correspond to the principal directions of the microstructure, z being along the direction of the gravity). We note K the average value of the three diagonal terms of $\mathbf{K}$, K_z its vertical component and K_{xy} the average of its two horizontal components.

TCD
6, 1157–1180, 2012

2.3 Computations of microstructural properties

Snow porosity (ϕ), and thus snow density ($\rho_s = \rho_i\,(1-\phi)$, in kg m^{-3}, with the ice density $\rho_i = 917$ kg m^{-3}), were estimated from 3-D images using a standard voxel counting algorithm.

The specific surface area (SSA, in m^2 kg^{-1}) of a snow sample is defined as the ratio of the total surface area of the air/ice interface per unit mass. It was computed from 3-D images using a stereological method as described by Flin et al. (2011) where the SSA is obtained by averaging SSA estimations computed along 3 orthogonal directions (x, y, z).

The equivalent sphere radius of a snow sample (r_{es}, in m) (Sommerfeld and Rocchio, 1993; Luciano and Albert, 2002), also called the optical radius (Picard et al., 2009), is a characteristic length of the ice grains at the microscopic scale. It corresponds to the radius of a collection of spheres having the same SSA value than the sample considered. r_{es} is related to SSA by $r_{es} = 3/(\mathrm{SSA}\times\rho_i)$.

3 Results and discussion

3.1 Dimensionless permeability vs. snow density

The permeability tensor **K**, the density ρ_s, and the SSA were computed on REVs. from the 35 3-D images. K exhibits values between 4×10^{-10} and 6×10^{-9} m^2, while ρ_s and SSA range from 103 to 544 kg m^{-3} and from 4 to 56 m^2 kg^{-1}, respectively. For each sample, detailed values are provided in Table 2 of the auxiliary online materials.

The intrinsic permeability is strongly linked to a characteristic length of the microstructure of the medium considered (Boutin and Geindreau, 2010). Thus, **K** is often normalized by its characteristic length to the square, leading to a dimensionless tensor that we note $\mathbf{K}^*$. Because snow SSA is a well-defined variable which is quite easy to estimate experimentally (Gallet et al., 2009; Arnaud et al., 2011), and numerically using 3-D

TCD
6, 1157–1180, 2012

images (Flin et al., 2011), we chose to use the equivalent sphere radius (r_{es}), directly given by the SSA computation, to normalize the components of **K**. In the following, $\mathbf{K}^*$ is thus equal to $\mathbf{K}/r_{es}^2$ and we keep the notation K^*, K_z^* and K_{xy}^* for the average, vertical and horizontal components of $\mathbf{K}^*$, respectively. One can also choose to normalize **K** by a characteristic length corresponding to the pore space and use the hydraulic radius (r_h), commonly applied to flow through pipes and open channels. This normalization is as good as that with r_{es}, since these two radii are linked by the simple relationship: $r_h = r_{es}(1-\phi)/(3\phi)$ (Bear, 1972). Computing the granulometry is another method to determine a characteristic length (Zermatten et al., 2011). However, this parameter is less convenient because it can not be estimated experimentally but only numerically from 3-D images.

Using the "T"-shape symbols, Fig. 1 shows the K_z^* and K_{xy}^* components, in logarithmic scale, as a function of density. K_z^*, K_{xy}^* and thus K^* decrease with increasing ρ_s. PP samples exhibit the largest values of K^* (1.05 for $\rho_s = 103\ \mathrm{kg\,m^{-3}}$), while the lowermost values are obtained for MF samples (2.16×10^{-3} for $\rho_s = 544\ \mathrm{kg\,m^{-3}}$). Differences between K_z^* and K_{xy}^* values can be observed for several samples, FC and DH notably, and will be presented in Sect. 3.5. The 35 values of K^* were fitted to ρ_s and provide the following regression: $K^* = 2.94 \times \exp(-0.013\rho_s)$ (black curve in Fig. 1), with a correlation coefficient of 0.985. This high coefficient indicates a strong relationship between **K**, SSA and ρ_s. The permeability K can thus be reasonably inferred from SSA and ρ_s using the fit given above.

3.2 Comparisons between numerical computations, models and fit

In addition to our computed values and fit, Fig. 1 displays four curves of the dimensionless permeability vs. ρ_s corresponding to the following regression, analytical formulas or numerical computations:

(i) The well-known Shimizu's fit (Shimizu, 1970) is expressed as:

$$K = 0.077D^2 \times \exp(-0.0078\rho_s), \quad \text{with } D = 2r_{es}$$

TCD
6, 1157–1180, 2012

(ii) The self consistent (SC) estimate was obtained assuming that the porous medium is constituted of a bicomposite spherical pattern made of an internal spherical grain and an external fluid shell that ensures fluid connectivity. The morphology of the porous medium is reduced to the most basic information, i.e. the porosity and the grain size. Using the SC method, Boutin (2000) showed that the above porous media lead to the following estimate:

$$K = [r_{es}^2/(3\beta^3)] \times [-1 + (2+\beta^5)/(\beta(3+2\beta^5))], \quad \text{where} \quad \beta = (1-\phi)^{(1/3)}$$

(iii) In the Carman-Kozeny (CK) model, the medium is treated as a bundle of capillarity tubes of equal length. By solving the Navier-Stokes equations simultaneously for all the channels passing through a cross-section normal to the flow in the porous medium, the permeability is written as $K = (c \times \phi^3)/(\mathrm{SSA_l} \times (1-\phi)^2)$ where $\mathrm{SSA_l}$ is the specific surface area per unit of ice volume ($\mathrm{SSA_l} = \mathrm{SSA} \times \rho_i$, in m^{-1}) and c a coefficient which characterizes the geometry of the channels in the model. Empirically, c is found to be equal to 0.2 for many types of porous media (Bear, 1972). The CK equation can thus be expressed as:

$$K = (4r_{es}^2 \times \phi^3)/(180(1-\phi)^2)$$

(iv) Numerical values of permeability of a simple cubic packing of spheres (Boutin and Geindreau, 2010) were also reported in Fig. 1.

Estimates of SC and CK models correspond fairly well to the computed data for a wide range of snow density, despite their simplified geometry (see Fig. 1). For the MF samples, models fail to reflect the snow microstructure and overestimate the permeability. These results can be explained by the fact that at low density the airflow around a snow particle is little affected by flow around its neighbours. In contrast, at higher density, snow particles are close together and the flow around one of them disturbs the flow around the others. This last phenomenon is not captured by analytical models.

TCD
6, 1157–1180, 2012

The Shimizu's fit and our computations are not in good agreement. As pointed out by several studies (Sommerfeld and Rocchio, 1993; Jordan et al., 1999), we believe that this difference is largely due to the method used by Shimizu (1970) to estimate grain size. From snow cross-sections, he computed a grain diameter $D = 2r_{es} = \sqrt{6\rho_s/\pi\rho_i n}$, where n, the number of ice grains appearing in the cross section per a unit area, is estimated by a counting process described as: "a complicated-shaped grain having m remarkable constrictions was counted as $m+1$ grains". This visual method is subjective and may lead to erroneous estimates of n and therefore of K^*.

Finally, we find that a simple cubic packing of spheres appears to be sufficient to provide a relationship of K^* vs. ρ_s roughly consistent with our results in the whole range of density considered, and notably for the MF samples.

3.3 Comparison to experimental and numerical data

Figure 2 allows a comparison between our 35 values of K^* (in black) and data from four previous studies (in color).

Sommerfeld and Rocchio (1993), Arakawa et al. (2009) and Courville et al. (2010) performed measurements of permeability using an air permeameter on fresh or equi-temperature snow, in south-eastern Wyoming (USA), on natural deposited dry snow in Hokkaido prefecture (Japan), and on polar firn (Antarctica), respectively. The SSA was estimated from photographs of snow section planes using a stereological method in the first two papers, while Courville et al. (2010) used tomographic images.

Numerical computations involving 3-D images were carried out in two recent studies: Courville et al. (2010) used Lattice-Boltzman modeling to compute the permeability in one direction on polar firn, and Zermatten et al. (2011) determined the vertical permeability for five snow samples using the direct pore-level simulations method. In both cases, SSA was estimated from the 3-D images.

TCD
6, 1157–1180, 2012

Data from these four studies are overall well consistent with our computations and both analytical models, showing a similar relationship of dimensionless permeability with ρ_s.

Experimental values, especially those from Arakawa et al. (2009) which provided the bigger dataset, are nevertheless more scattered than computed values. This can be explained by the large number of experimental data but also by the difficulty to make reliable and reproducible measurements of permeability. A first source of errors may be the physical damage of the sample caused during its sampling or its handling (Sommerfeld and Rocchio, 1993). Shimizu (1970) and Sommerfeld and Rocchio (1993) also pointed out a bias linked to possible condensation/sublimation of the snow microstructure induced by the airflow imposed through the snow sample during the measurement.

The computations of Courville et al. (2010), Zermatten et al. (2011) and this study are in excellent agreement, although all three studies use different numerical methods and boundary conditions on the external faces of the sample. Zermatten et al. (2011) indicate significant differences between the CK model and their values, while Fig. 2 shows a good agreement between both: they apparently plotted an erroneous CK equation, using the specific surface area per unit of snow volume (SSA_V, in m^{-1}) in the expression of $K = \phi^3/(5(1-\phi)^2 SSA_I^2)$ instead of SSA_I (see Sect. 3.2).

3.4 Representative elementary volume

The Representative Elementary Volume (REV) can be estimated by calculating values of a given variable from several sub-volumes of increasing sizes. It is reached as soon as values do not vary significantly when sub-volumes of computation increase. Note that the REV size depends on the variable and on the sample studied: REVs. with respect to snow permeability are generally equal or larger than those for other variables, such as ρ_s, SSA or the effective thermal conductivity (Flin et al., 2011; Calonne et al., 2011). Thus, a special attention must be paid to ensure that computations are carried out on a sufficiently large volume.

TCD
6, 1157–1180, 2012

Estimations of the REV were performed on one sample of each snow type and range from 2.5 mm^3 for the PP sample to 5.5 mm^3 for the MF sample (see auxiliary online materials), which corresponds to the total volumes of our 3-D images or less.

For 3 snow samples (RG, FC and MF), computations of **K**, SSA and ρ_s were performed on total volumes and on sub-volumes of different sizes. Figure 3 shows the obtained values of K^* as a function of ρ_s. By increasing the volume size of calculation (from volume 1 to 4 or 5 in Fig. 3), the result becomes closer to the previous one, which is consistent with the REV definition. Overall, our computed values are roughly consistent with our fit and the CK and SC model. Thus, we point out the fact that if **K**, SSA and/or ρ_s are computed on a volume smaller than their REV, the final result, i.e. K^* vs. ρ_s, remains in agreement with the evolution of K^* proposed by our fit or analytical models. This observation highlights the robustness of the relationship between **K**, SSA and ρ_s.

3.5 Anisotropy

Numerical estimations of the permeability tensor allow to compute, for each sample, the anisotropy coefficient of **K** such as $A(\mathbf{K}) = K_z/K_{xy}$. As shown in Fig. 5, $A(\mathbf{K})$ ranges from 0.74 for a PP sample collected in the field, to 1.66 for a particularly evolved DH sample obtained in cold room. For this last sample, the velocity of the airflow along the vertical and horizontal directions is illustrated in Fig. 4 (see left and right hand side, respectively). The flow, constrained by the snow microstructure, is clearly more intense in the vertical than in the horizontal direction, leading to a high K_z value. The value of 1.66 is of the same order of magnitude as the analytical coefficient of anisotropy for a network of vertical cylinders (Boutin, 2000). The range in $A(\mathbf{K})$ is consistent with the values between 0.75 and 1.9 measured by Luciano and Albert (2002) on firn collected from 1 to 13 m depth at Summit, Greenland.

Similarly, by defining the anisotropy coefficient $A(\mathbf{k}_{\text{eff}})$ of the effective thermal conductivity tensor $\mathbf{k}_{\text{eff}}$ provided in Calonne et al. (2011), one can compare $A(\mathbf{K})$ to $A(\mathbf{k}_{\text{eff}})$

TCD
6, 1157–1180, 2012

for the same snow samples. According to Fig. 5, the anisotropy coefficients considered are in good agreement, showing that the microstructure influences similarly both variables. Nevertheless, some discrepancies can be observed depending on density, snow type and microstructure.

4 Conclusions

The intrinsic permeability tensor **K** was computed on 35 tomographic images of various snow types by solving numerically on a REV a specific boundary value problem arising from the homogenization process. As the permeability is related to a characteristic length of the microstructure, we chose the equivalent sphere radius to reduce **K** to a dimensionless tensor $\mathbf{K}^*$. This variable is convenient because it is directly inferred from the specific surface area (SSA) of the snow sample which can be computed using 3-D images, as performed in this study, and also measured experimentally.

Values of K^*, average of vertical and horizontal components of $\mathbf{K}^*$, plotted as a function of snow density (ρ_s), were presented and a fit was proposed, leading to two main observations: (i) Our relationship of K^* vs. ρ_s is fairly consistent with that of analytical models and data of the literature. (ii) K^* and ρ_s are strongly correlated. It leads to the major conclusion that the permeability of seasonal snow, if assumed isotropic, can be reasonably inferred from its ρ_s and SSA field measurements using the proposed fit. This is particularly useful for numerical models able to simulate ρ_s and SSA, allowing a straightforward estimate of snow permeability, with a great potential, e.g. for applications involving snowpack ventilation, such as air/snow chemical exchanges. Vertical and horizontal components of **K** were used to compute the anisotropy coefficient of each sample. It was shown that anisotropy coefficients of **K** and of the thermal conductivity tensor are consistent and allow to differentiate the DH and FC samples (highest values) from other snow types. This result suggests that the permeability may be helpful for quantitative classification of snow, as proposed by Arakawa et al. (2009),

TCD
6, 1157–1180, 2012

provided that its anisotropy can be measured. However, the high coefficient of correlation found between **K**, SSA and ρ_s seems to prevent the use of the permeability as an independent state variable of snow.

Supplementary material related to this article is available online at: http://www.the-cryosphere-discuss.net/6/1157/2012/tcd-6-1157-2012-supplement.pdf.

Acknowledgements. Funding by Météo-France, INSU-LEFE and DigitalSnow (ANR-11-BS02-009) is acknowledged. We thank scientists of the ESRF ID19 beamline (J. Baruchel, E. Boller, W. Ludwig, X. Thibault) and of the 3S-R laboratory (J. Desrues), where the 3-D images were obtained. We also thank CEN staff for technical support, F. Domine (Takuvik International Laboratory) for stimulating discussions and H. Arakawa (YAGAI-KAGAKU Co., Ltd) for providing us his dataset.

The publication of this article is financed by CNRS-INSU.

References

Akitaya, E.: Studies of depth hoar, Low. Temp. Sci., Series A, 26, 1–67, 1974. 1159

Albert, M. R.: Effects of snow and firn ventilation on sublimation rates, Ann. Glaciol., 35, 52–56, doi:10.3189/172756402781817194, http://www.ingentaconnect.com/content/igsoc/agl/2002/00000035/00000001/art00010, 2002. 1159, 1162

TCD
6, 1157–1180, 2012

Albert, M., Shuman, C., Courville, Z., Bauer, R., Fahnestock, M., and Scambos, T.: Extreme firn metamorphism: impact of decades of vapor transport on near-surface firn at a low-accumulation glazed site on the East Antarctic plateau, Ann. Glaciol., 39, 73–78, doi:10.3189/172756404781814041, http://www.ingentaconnect.com/content/igsoc/agl/2004/00000039/00000001/art00013, 2004. 1159

Arakawa, H., Izumi, K., Kawashima, K., and Kawamura, T.: Study on quantitative classification of seasonal snow using specific surface area and intrinsic permeability, Cold. Reg. Sci. Technol., 59, 163–168, doi:10.1016/j.coldregions.2009.07.00, 2009. 1159, 1166, 1167, 1169

Arnaud, L., Picard, G., Champollion, N., Domine, F., Gallet, J.-C., Lefebvre, E., Fily, M., and Barnola, J.-M.: Measurement of vertical profiles of snow specific surface area with a 1 cm resolution using infrared reflectance: instrument description and validation, J. Glaciol., 57, 17–29, doi:10.3189/002214311795306664, http://www.ingentaconnect.com/content/igsoc/jog/2011/00000057/00000201/art00002, 2011. 1163

Auriault, J.: Heterogeneous periodic and random media, Are the equivalent macroscopic descriptions similar?, Int. J. Eng. Sci., 49, 806–808, 2011. 1161

Auriault, J.-L.: Heterogeneous Medium. Is an Equivalent Description Possible?, Int. J. Eng. Sci., 29, 785–795, 1991. 1161

Auriault, J.-L., Boutin, C., and Geindreau., C.: Homogenization of coupled phenomena in heterogenous media, Wiley-ISTE, London, 2009. 1159, 1161

Bader, H.: Mineralogische und strukturelle Charakterisierung des Schnees und seiner Metamorphose, in: Der Schnee und seine Metamorphose, edited by: Bader, H., Haefeli, R., Buchker, E., Neher, J., Eckel, O., and Thams, C., Kümmerly & Frey, Bern, Beiträge zur Geologie der Schweiz, Geotechnische Serie Hydrologie, 3, 1–61, 1939. 1159

Bear, J.: Dynamics of Fluids in Porous Media, Dover, Chapter 5: The equation of motion of homgeneous fluid, 165–167, 1972. 1164, 1165

Boutin, C.: Study of Permeability by Periodic and Self Consistent Homogenisation, Eur. J. Mech. A/Solids, 19, 603–632, 2000. 1165, 1168

Boutin, C. and Geindreau, C.: Periodic homogenization and consistent estimates of transport parameters through sphere and polyhedron packings in the whole porosity range, Phys. Revi. E, 82, 036313-1–036313-18, doi:10.1103/PhysRevE.82.036313, 2010. 1163, 1165

Brun, E. and Touvier, F.: Etude expérimentale de la convection thermique dans la neige, J. Phys.-Paris, 48, 257–262, 1987. 1159

Brzoska, J.-B., Coléou, C., Lesaffre, B., Borel, S., Brissaud, O., Ludwig, W., Boller, E., and

TCD
6, 1157–1180, 2012

Baruchel, J.: 3D visualization of snow samples by microtomography at low temperature, ESRF Newsletter, 32, 22–23, 1999. 1159
Calonne, N., Flin, F., Morin, S., Lesaffre, B., du Roscoat, S. R., and Geindreau, C.: Numerical and experimental investigations of the effective thermal conductivity of snow, Geophys. Res. Lett., 38, L23501, http://dx.doi.org/10.1029/2011GL049234, 2011. 1159, 1167, 1168
Colbeck, S. C.: A theory for water flow through a layered snowpack, Water Resour. Res., 11, 261–266, http://dx.doi.org/10.1029/WR011i002p00261, 1975. 1159
Colbeck, S. C.: An analysis of water flow in dry snow, Water Resour. Res., 12, 523–527, http://dx.doi.org/10.1029/WR012i003p00523, 1976. 1159
Colbeck, S. C.: Air movement in snow due to windpumping, J. Glaciol., 35, 209–213, 1989. 1158
Colbeck, S. C.: A model of wind pumping for layered snow, J. Glaciol., 43, 60–65, 1997. 1158
Coléou, C., Lesaffre, B., Brzoska, J.-B., Ludwig, W., and Boller, E.: Three-dimensional snow images by X-ray microtomography, Ann. Glaciol., 32, 75–81, doi:10.3189/172756401781819418, 2001. 1159, 1160
Courville, Z., Hörhold, M., Hopkins, M., and Albert, M.: Lattice-Boltzmann modeling of the air permeability of polar firn, J. Geophys. Res., 115, F04032, doi:10.1029/2009JF001549, http://dx.doi.org/10.1029/2009JF001549, 2010. 1159, 1166, 1167
Ene, H. and Sanchez-Palencia, E.: Equations et Phénomènes de Surface Pour Écoulement Dans un Modèle de Milieu Poreux, J. de Mécanique, 14, 73–108, 1975. 1161
Fierz, C., Armstrong, R. L., Durand, Y., Etchevers, P., Greene, E., McClung, D. M., Nishimura, K., Satyawali, P. K., and Sokratov, S. A.: The international classification for seasonal snow on the ground, IHP-VII Technical Documents in Hydrology n 83, IACS Contribution n 1, 2009. 1160, 1176, 1177, 1178, 1180
Flin, F. and Brzoska, J.-B.: The temperature gradient metamorphism of snow: vapour diffusion model and application to tomographic images, Ann. Glaciol., 49, 17–21, doi:10.3189/172756408787814834, 2008. 1160
Flin, F., Brzoska, J.-B., Lesaffre, B., Coléou, C., and Pieritz, R. A.: Three-dimensional geometric measurements of snow microstructural evolution under isothermal conditions, Ann. Glaciol., 38, 39–44, doi:10.3189/172756404781814942, 2004. 1160
Flin, F., Lesaffre, B., Dufour, A., Gillibert, L., Hasan, A., Rolland du Roscoat, S., Cabanes, S., and Pugliese, P.: On the Computations of Specific Surface Area and Specific Grain Contact Area from Snow 3D Images, in: P. C. I., edited by: Furukawa, Y., Hokkaido University Press,

TCD
6, 1157–1180, 2012

Sapporo, JP, proceedings of the 12th International Conference on the Physics and Chemistry of Ice held at Sapporo, Japan on 5–10 September 2010, 321–328, 2011. 1160, 1163, 1164, 1167

Freitag, J., Dobrindt, U., and Kipfstuhl, J.: A new method for predicting transport properties of polar firn with respect to gases on the pore-space scale, Ann. Glaciol., 35, 538–544, doi:10.3189/172756402781816582, http://www.ingentaconnect.com/content/igsoc/agl/2002/00000035/00000001/art00086, 2002. 1159

Freitag, J., Wilhelms, F., and Kipfstuhl, S.: Microstructure-dependent densification of polar firn derived from X-ray microtomography, J. Glaciol., 50, 243–250, doi:10.3189/172756504781830123, http://www.ingentaconnect.com/content/igsoc/jog/2004/00000050/00000169/art00009, 2004. 1159

Gallet, J.-C., Domine, F., Zender, C. S., and Picard, G.: Measurement of the specific surface area of snow using infrared reflectance in an integrating sphere at 1310 and 1550 nm, The Cryosphere, 3, 167–182, doi:10.5194/tc-3-167-2009, 2009. 1163

Grannas, A. M., Jones, A. E., Dibb, J., Ammann, M., Anastasio, C., Beine, H. J., Bergin, M., Bottenheim, J., Boxe, C. S., Carver, G., Chen, G., Crawford, J. H., Dominé, F., Frey, M. M., Guzmán, M. I., Heard, D. E., Helmig, D., Hoffmann, M. R., Honrath, R. E., Huey, L. G., Hutterli, M., Jacobi, H. W., Klán, P., Lefer, B., McConnell, J., Plane, J., Sander, R., Savarino, J., Shepson, P. B., Simpson, W. R., Sodeau, J. R., von Glasow, R., Weller, R., Wolff, E. W., and Zhu, T.: An overview of snow photochemistry: evidence, mechanisms and impacts, Atmos. Chem. Phys., 7, 4329–4373, doi:10.5194/acp-7-4329-2007, 2007. 1159

Hörhold, M. W., Albert, M. R., and Freitag, J.: The impact of accumulation rate on anisotropy and air permeability of polar firn at a high-accumulation site, J. Glaciol., 55, 625–630, doi:10.3189/002214309789471021, http://www.ingentaconnect.com/content/igsoc/jog/2009/00000055/00000192/art00005, 2009. 1159

Jordan, R. E., Hardy, J. P., Perron, F. E., and Fisk, D. J.: Air permeability and capillary rise as measures of the pore structure of snow: an experimental and theoretical study, Hydrol. Proc., 13, 1733–1753, doi:10.1002/(SICI)1099-1085(199909)13:12/13¡1733::AID-HYP863¿3.0.CO;2-2, 1999. 1159, 1166

Kaempfer, T. U., Schneebeli, M., and Sokratov, S. A.: A microstructural approach to model heat transfer in snow, Geophys. Res. Lett., 32, L21503, doi:10.1029/2005GL023873, 2005. 1159

Katsushima, T., Kumakura, T., and Takeuchi, Y.: A multiple snow layer model including a parameterization of vertical water channel process in snowpack, Cold Reg. Sci. Technol., 59,

TCD
6, 1157–1180, 2012

143–151, http://linkinghub.elsevier.com/retrieve/pii/S0165232X09001499, 2009. 1159
Koivu, V., Decain, M., Geindreau, C., Mattila, K., Bloch, J.-F., and Kataja, M.: Transport properties of heterogeneous materials, Combining computerised X-ray micro-tomography and direct numerical simulations, Inte. Comput. Fluid Dyn., 10, 713–721, 2009. 1159
Luciano, G. L. and Albert, M. R.: Bidirectional permeability measurements of polar firn, Ann. Glaciol., 35, 63–66, doi:10.3189/172756402781817095, http://www.ingentaconnect.com/content/igsoc/agl/2002/00000035/00000001/art00012, 2002. 1163, 1168
Mei, C. C. and Auriault, J. L.: The Effect of Inertia on Flow Through Porous Medium, J. Fluid. Mech., 222, 647–663, 1991. 1162
Neumann, T. A.: Effects on firn ventilation on Geochemistry of polar snow, Phd thesis, University of Washington, 2003. 1159
Picard, G., Brucker, L., Fily, M., Gallée, H., and Krinner, G.: Modeling time series of microwave brightness temperature in Antarctica, J. Glaciol., 55, 537–551, 2009. 1163
Powers, D., O'Neill, K., and Colbeck, S. C.: Theory of Natural Convection in Snow, J. Geophys. Res., 90, 10641–10649, http://dx.doi.org/10.1029/JD090iD06p10641, 1985. 1159
Raymond, C. and Tusima, K.: Grain coarsening of water-saturated snow, J. Glaciol., 22, 83–105, 1979. 1160
Schneebeli, M. and Sokratov, S. A.: Tomography of temperature gradient metamorphism of snow and associated changes in heat conductivity, Hydrol. Process., 18, 3655–3665, doi:10.1002/hyp.5800, 2004. 1159
Shimizu, H.: Air permeability of deposited snow, Contributions from the Institute of Low Temperature Science, A22, 1–32, http://eprints.lib.hokudai.ac.jp/dspace/handle/2115/20234, 1970. 1159, 1164, 1166, 1167
Sommerfeld, R. A. and Rocchio, J. E.: Permeability measurements on new and equitemperature snow, Water Resour. Res., 29, 2485–2490, http://dx.doi.org/10.1029/93WR01071, 1993. 1159, 1163, 1166, 1167
Sturm, M. and Johnson, J. B.: Natural Convection in the Subarctic Snow Cover, J. Geophys. Res., 96, 11657–11671, http://dx.doi.org/10.1029/91JB00895, 1991. 1159
Thoemen, H., Walther, T., and Wiegmann, A.: 3D simulation of macroscopic heat and mass transfer properties from the microstructure of wood fibre networks, Comp. Sci. Techn., 68, 608–616, doi:10.1016/j.compscitech.2007.10.014, 2008. 1159
Waldner, P. A., Schneebeli, M., Schultze-Zimmermann, U., and Fühler, H.: Effect of snow structure on water flow and solute transport, Hydrol. Proc., 18, 1271–1290, http://doi.wiley.

TCD
6, 1157–1180, 2012

com/10.1002/hyp.1401, 2004. 1159
Yamaguchi, S., Katsushima, T., Sato, A., and Kumakura, T.: Water retention curve of snow with different grain sizes, Cold Reg. Sci. Technol., 64, 87–93, doi:10.1016/j.coldregions.2010.05.008, http://www.sciencedirect.com/science/article/pii/S0165232X1000114X, international Snow Science Workshop 2009 Davos, 2010. 1159
Zermatten, E., Haussener, S., Schneebeli, M., and Steinfeld, A.: Tomography-based determination of permeability and DupuitForchheimer coefficient of characteristic snow samples, J. Glaciol., 57, 811–816, doi:10.3189/002214311798043799, http://www.ingentaconnect.com/content/igsoc/jog/2011/00000057/00000205/art00004, 2011. 1159, 1164, 1166, 1167

TCD
6, 1157–1180, 2012

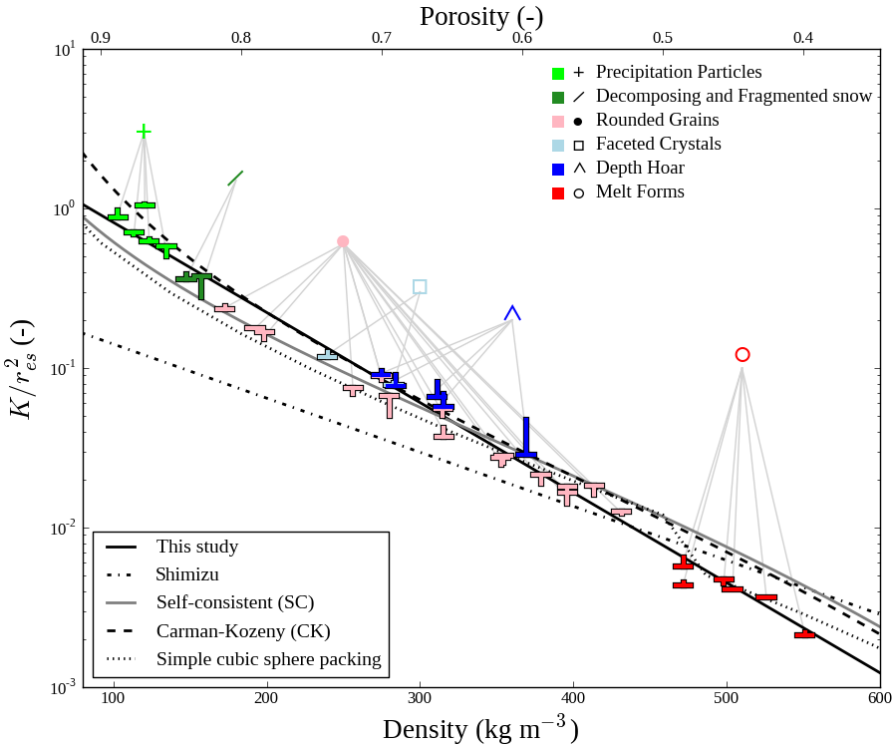

Fig. 1. Dimensionless permeability vs. snow density. "T" symbols indicate the computation values. Tips and horizontal bars of the "T" shapes represent the vertical and horizontal components of $\mathbf{K}^*$, as computed in our study, respectively. Colors correspond to the ICSSG (Fierz et al., 2009). Analytical models, numerical computations and fits are also plotted.

TCD
6, 1157–1180, 2012

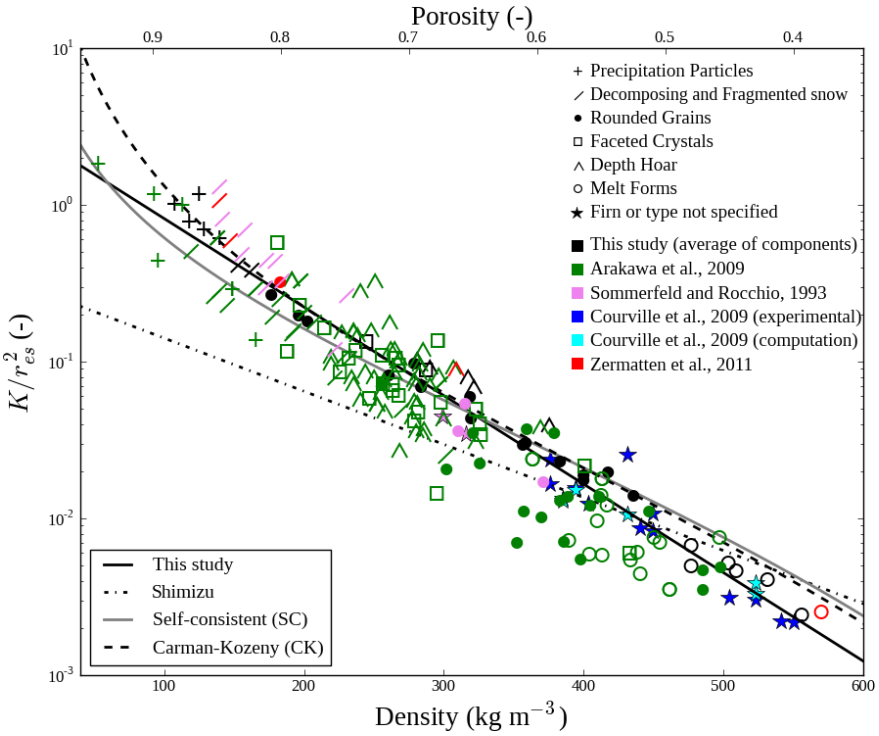

Fig. 2. Dimensionless permeability vs. snow density. Our K^* values (in black) are compared to results from other studies (in color). Symbols correspond to the ICSSG (Fierz et al., 2009), excepting stars which are used when firn is considered or when the snow type is not specified in the paper. Analytical models and fits are also plotted.

TCD
6, 1157–1180, 2012

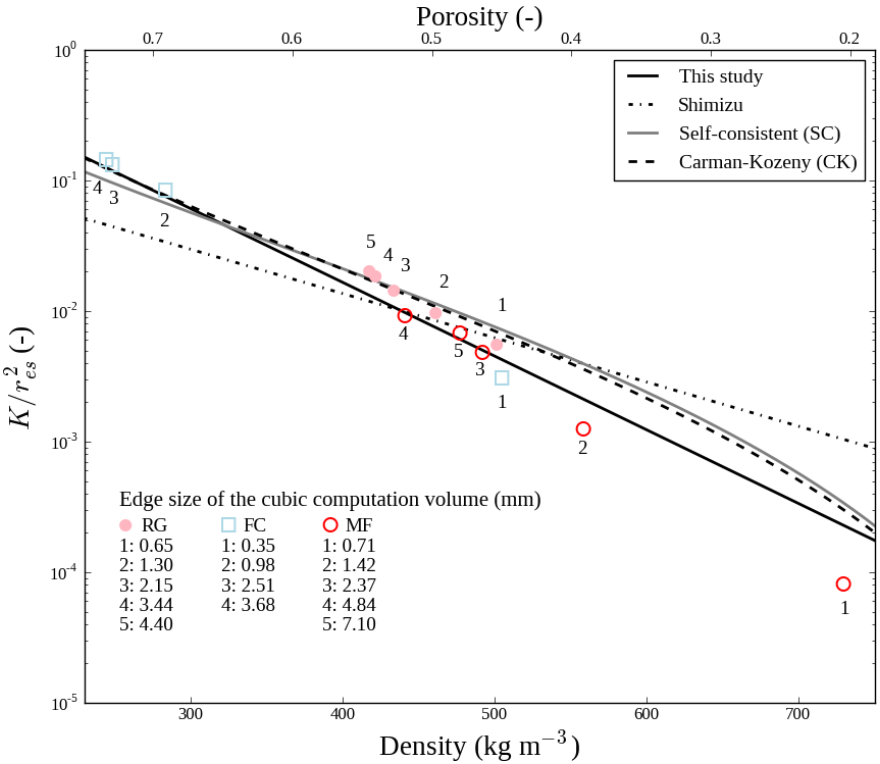

Fig. 3. Dimensionless permeability versus snow density for 3 snow samples. Symbols and colors correspond to the ICSSG (Fierz et al., 2009). For a given sample, each symbol represents a particular volume from which **K**, SSA and ρ_s were computed. The largest volume corresponds to the total volume of the sample. Analytical models and fits are also plotted.

TCD
6, 1157–1180, 2012

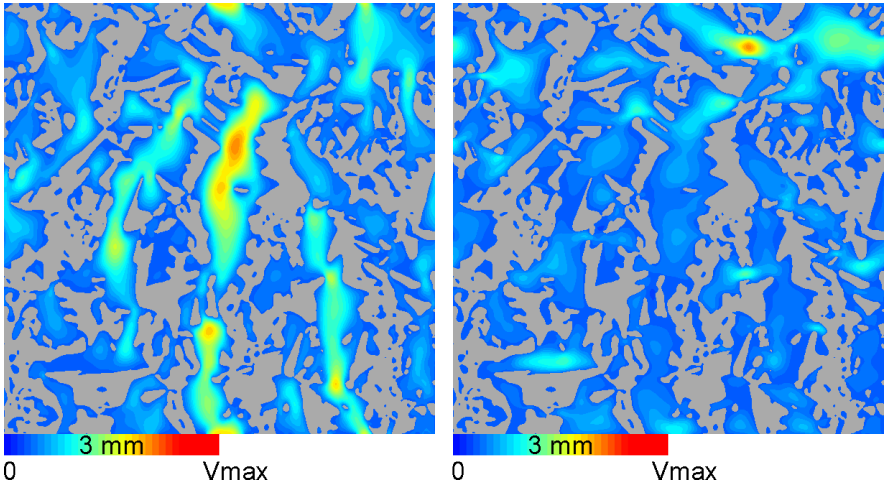

Fig. 4. Vertical cross section (plane (y,z)) of an evolved DH sample: Airflow velocity at the pore scale induced by a macroscopic gradient of pressure along the z (left) and y (right) direction. Ice grains are represented in gray. In the pores, colors indicate the velocity increasing from dark blue to red.

TCD
6, 1157–1180, 2012

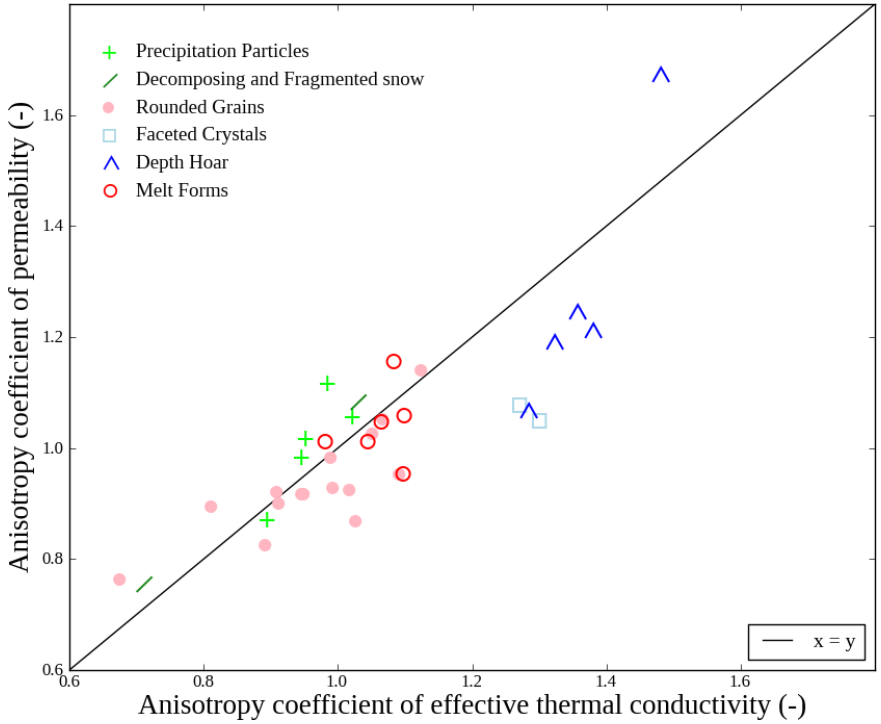

Fig. 5. $A(\mathbf{K})$ versus $A(\mathbf{k}_{\mathbf{eff}})$. Symbols and colors correspond to the ICSSG (Fierz et al., 2009).

TCD
6, 1157–1180, 2012